



Pergamon

Available online at [www.sciencedirect.com](http://www.sciencedirect.com)

SCIENCE @ DIRECT®

Acta Materialia 51 (2003) 4751–4760



[www.actamat-journals.com](http://www.actamat-journals.com)

# Effect of Mg addition on the creep and yield behavior of an Al–Sc alloy

Emmanuelle A. Marquis \*, David N. Seidman, David C. Dunand

*Department of Materials Science and Engineering, Northwestern University, Evanston, IL 60208-3108, USA*

Received 5 March 2003; received in revised form 19 May 2003; accepted 22 May 2003

## Abstract

The relationships between microstructure and strength were studied at room temperature and 300 °C in an Al–2 wt% Mg–0.2 wt% Sc alloy, containing Mg in solid-solution and Al<sub>3</sub>Sc (L1<sub>2</sub> structure) as nanosize precipitates. At room temperature, the yield strength is controlled by the superposition of solid-solution and precipitation strengthening. At 300 °C and at large applied stresses, the creep strength, which is characterized by a stress exponent of ~5, is significantly improved compared to binary Al–Sc alloys, and is independent of the size of the Al<sub>3</sub>Sc precipitates. At small applied stress, a threshold stress exists, increasing from 9% to 70% of the Orowan stress with increasing Al<sub>3</sub>Sc precipitate radius from 2 to 25 nm. An existing model based on a climb-controlled bypass mechanism is in semi-quantitative agreement with the precipitate radius dependence of the threshold stress. The model is, however, only valid for coherent precipitates, and the Al<sub>3</sub>Sc precipitates lose coherency for radii larger than 11 nm. For semi-coherent precipitates with radii greater than 15 nm, the threshold stress remains high, most likely because of the presence of interfacial misfit dislocations.

© 2003 Acta Materialia Inc. Published by Elsevier Ltd. All rights reserved.

*Keywords:* Transmission electron microscopy; Aluminum alloys; Coarsening; Creep; Al<sub>3</sub>Sc precipitates

## 1. Introduction

The combination of solid-solution strengthening and precipitation strengthening has been well characterized with respect to the room temperature

strength of alloys [1]. The creep properties of Al–Sc alloys containing low volume fractions of Al<sub>3</sub>Sc precipitates exhibit significant improvement compared to pure Al with the presence of a threshold stress of the order of 20–30 MPa, due to precipitate/dislocation interactions [2]. The creep behavior of Al–Mg solid-solutions is extensively described in the literature [3–7]. The synergy of solid-solution strengthening and precipitate strengthening has, however, not been extensively studied at elevated temperatures. Several authors [8,9] have discussed the differences between Al-based and Al–Mg based particle-reinforced alloys.

\* Corresponding author. Present address: Thin Film and Interface Department, Sandia National Laboratories, Livermore, CA 94550-9161, USA. Tel.: +1-925-294-3287; fax: +1-925-294-3231.

*E-mail addresses:* [emarqui@sandia.gov](mailto:emarqui@sandia.gov) (E.A. Marquis); [id-seidman@northwestern.edu](mailto:id-seidman@northwestern.edu) (D.N. Seidman); [dunand@northwestern.edu](mailto:dunand@northwestern.edu) (D.C. Dunand).

Results on oxide dispersion strengthened alloys demonstrated that a threshold stress arises from the presence of particles [9]; for stresses greater than the threshold stress, viscous glide of dislocations does not contribute to the strength of the Al–Mg based particle-reinforced alloys, which appear weaker than the Al–Mg unreinforced alloy [9]. Studies on Al–5% Mg–0.5% Fe and Al–5% Mg–6.4% Ni showed that the strengthening effects from the precipitates depend on their shape and size; small  $\text{Al}_6\text{Fe}$  precipitates are ineffective compared to the Mg solid-solution strengthening, whereas rod-like  $\text{Al}_3\text{Ni}$  precipitates give rise to a threshold stress [10]. Different creep behaviors have been reported, depending on precipitate morphology, and volume fraction. The contribution of the present research is to describe the combined effects of Mg in solid-solution and Sc in coherent  $\text{Al}_3\text{Sc}$  spheroidal precipitates on the strengthening at ambient (yield regime) and elevated (creep regime) temperatures.

## 2. Experimental procedures

The Al–2 wt% Mg–0.2 wt% Sc alloy was prepared by casting 99.9% purity Al and Mg with an Al–0.5 wt% Sc master alloy to a graphite mold. The Al–Mg–Sc ingots were re-melted in a steel crucible coated with graphite and directional solidification was obtained by means of a copper rod placed at the bottom of the furnace in contact with the crucible during solidification. This copper rod, extending outside the heated zone, acted as a heat extractor. Solidification was performed under 1.5 atm of argon. With this procedure, the amount of porosity was reduced to less than 0.5%, as determined by the Archimedes method. The alloy was homogenized at 617 °C for 24 h, quenched into room temperature water and aged between 300 and 450 °C for times varying from 0.5 to 280 h.

Vickers microhardness was measured on polished samples using the average value of 20 independent measurements made on several grains. Compression creep experiments were performed to avoid any effect of residual porosity in the Mg-containing alloys on creep behavior, due to the broad solidification range caused by the addition

of Mg. Creep experiments were performed on cylindrically shaped specimens (10 mm in diameter and 22 mm in height) under constant load, corresponding to compressive stresses in the range 5–70 MPa, and at constant temperature (225–300 °C) in air. A superalloy compression cage was employed with platens lubricated with boron nitride to limit friction at the extremities of the sample. Connecting rods were also lubricated with boron nitride to limit friction in the cage itself. Displacements of the platens were transmitted to a linear variable differential transducer using an extensometer. After steady-state deformation was achieved, the load was increased, resulting in three to five data points per specimen.

Transmission electron microscopy (TEM) samples were prepared by cutting 350  $\mu\text{m}$  thick foils from aged specimens. Three millimeter diameter disks were punched from the foil, mechanically ground to 200  $\mu\text{m}$ , and then jet electropolished (Struers Tenupol) with a solution of 5 vol% perchloric acid in methanol at –30 °C, using a bath of dry ice in methanol. TEM observations were performed utilizing an Hitachi 8100 microscope operating at 200 kV.

## 3. Results

### 3.1. Microstructure

The ternary alloy exhibits very coarse and elongated grains (Fig. 1) and, after aging, high number densities of coherent  $\text{Al}_3\text{Sc}$  precipitates with the  $\text{L}1_2$  structure were observed. TEM images in Fig. 2 exhibit decreasing number densities and increasing average radius of the  $\text{Al}_3\text{Sc}$  precipitates, obtained after aging at 300 °C for 24 h with further aging at 400 °C for 0, 2, 10, 24, 72, or 240 h. In the specimens aged at 400 °C for 24 h ( $\langle r \rangle = 10.5$  nm), some interfacial dislocations are observed at the matrix/precipitate interface for the largest precipitates, however, most of the precipitates remain coherent. The proportion of large precipitates with interfacial dislocations becomes more important after aging at 400 °C for 72 h ( $\langle r \rangle = 13.4$  nm). And after aging at 400 °C for 240 h ( $\langle r \rangle = 19.5$  nm), all the  $\text{Al}_3\text{Sc}$  precipitates have lost their coherency

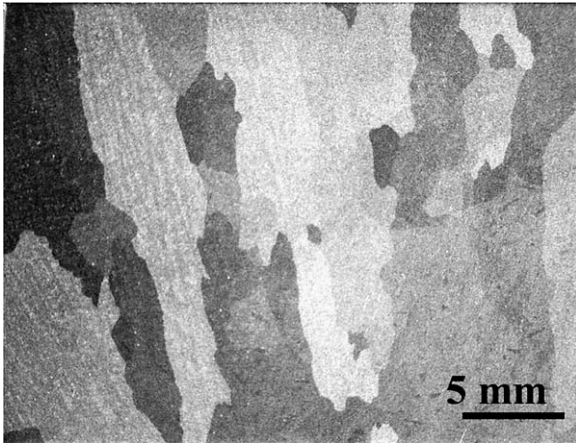


Fig. 1. Optical micrograph of an Al-2 wt% Mg-0.2 wt% Sc alloy exhibiting very large elongated grains.

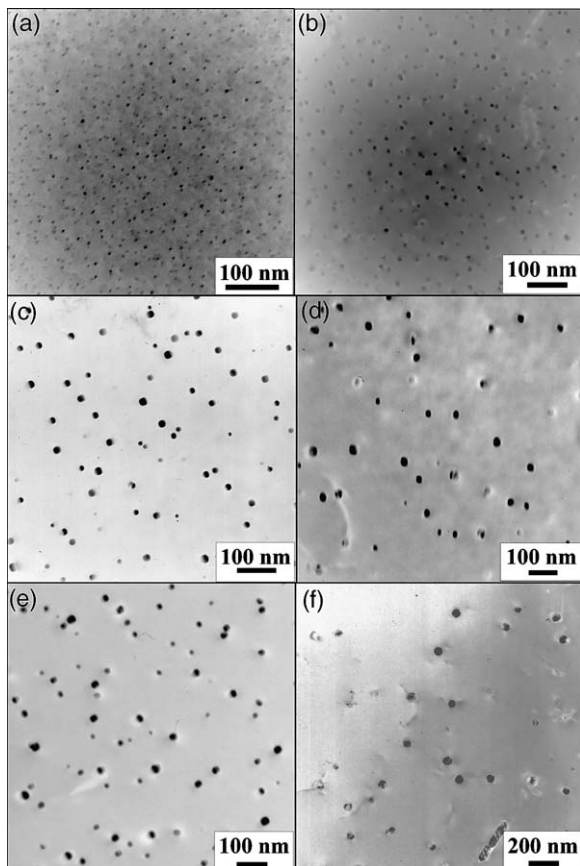


Fig. 2. TEM micrographs of  $\text{Al}_3\text{Sc}$  precipitates obtained after pre-aging at 300 °C for 24 h followed by aging at 400 °C for (a) 0 h, (b) 2 h, (c) 10 h, (d) 24 h, (e) 72 h, and (f) 240 h.

and interfacial misfit dislocations are observed, as shown in Fig. 3. The precipitate/matrix interface thus remains coherent for precipitate radii up to  $r \approx 15$  nm.

### 3.2. Microhardness

The Vickers microhardness value of the as-quenched alloy is  $430 \pm 10$  MPa. The aging response of the alloy, measured from changes in Vickers microhardness after aging at 300 and 350 °C for various times (Fig. 4), exhibits four different regions: (a) an incubation period of decreasing duration with increasing temperature; (b) a short transient period with a rapid increase in hardness values (under-aging); (c) a plateau at high hardness values (peak aging); and (d) decreasing hardness values with increasing aging times (overaging). The value of the peak hardness, and the time for achieving and departing from peak hardness all decrease as the temperature is increased from 300 to 350 °C.

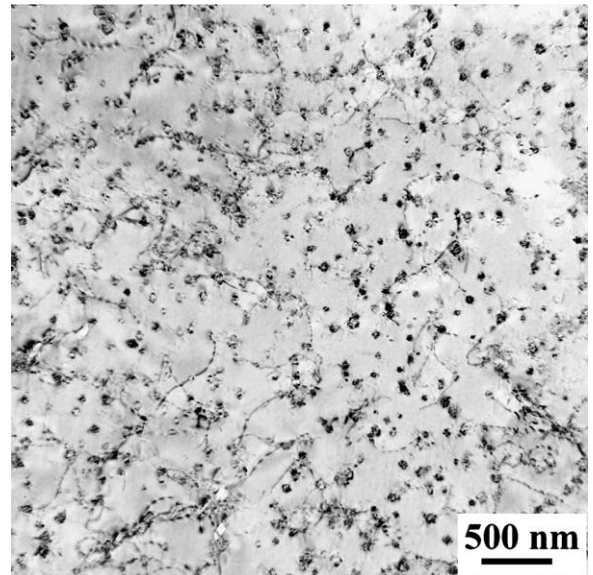


Fig. 3. Dark-field TEM micrograph showing dislocation contrast as observed in the ternary alloy after aging at 300 °C for 24 h followed by 400 °C for 240 h,  $r = 19.5$  nm.

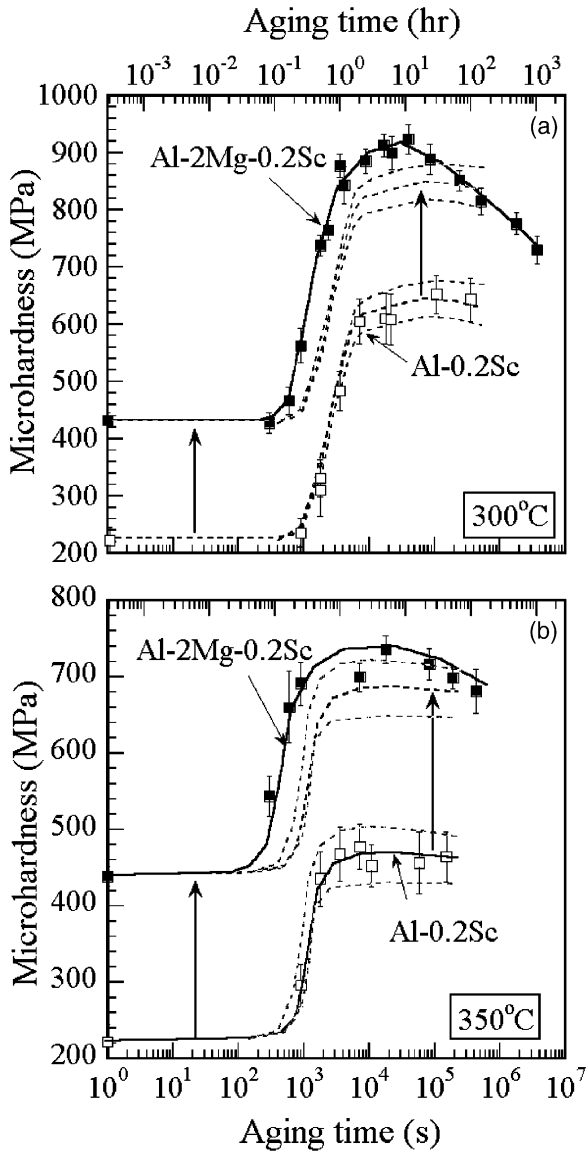


Fig. 4. Vickers microhardness as a function of aging time for Al-0.2 wt% Sc (open squares, from Ref. [2]) and Al-2 wt% Mg-0.2 wt% Sc (solid squares) at (a) 300 °C and (b) 350 °C. The dashed lines correspond to the curves for the Al-0.2 wt% Sc alloy translated upward by 220 MPa.

### 3.3. Creep properties

The creep behavior of the ternary alloy is characterized by high stress exponents ( $n \cong 40$ ), decreasing to lower values of about  $n \cong 5$  at higher

stresses (Fig. 5). For all heat-treatments utilized, the creep strength of Al-2 wt% Mg-0.2 wt% Sc alloy is significantly improved compared to that of pure aluminum. Fig. 5 also compares the creep behavior at 300 °C of the Al-2 wt% Mg-0.2 wt% Sc alloy with an Al-0.2 wt% Sc binary alloy, reported on in Ref. [2]. At low stresses, the creep resistance of the ternary alloy aged at 300 °C for 24 h is comparable to that of the Al-Sc binary alloy for the same aging treatment. Comparing the behavior of the ternary alloy to that of the precipitate-free Al-2 wt% Mg binary alloy (Fig. 6), the presence of Al<sub>3</sub>Sc precipitates dramatically increases the creep resistance in the low-stress region through a threshold stress, below which creep is not measurable. The creep threshold stress increases with precipitate radius in the range of 20–30 MPa. At large applied stresses, the strain rate of the ternary alloy is lower than that of the Al-2 wt% Mg binary alloy by one order of magnitude, and it is insensitive to the precipitate radius.

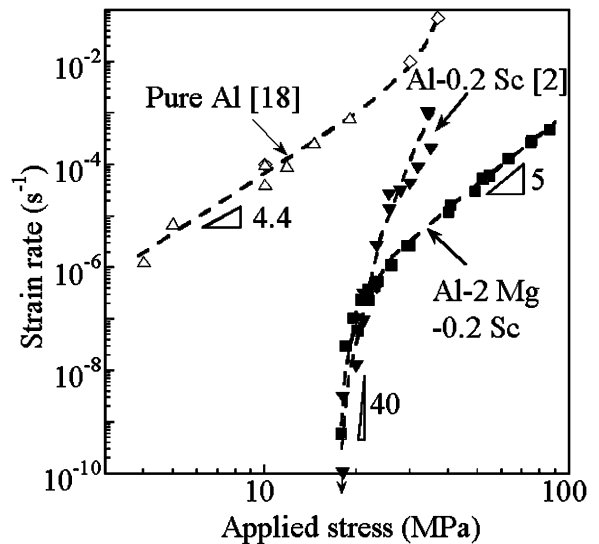


Fig. 5. Strain rate versus applied stress curves at 300 °C, comparing the creep behaviors of pure Al [18], Al-0.2 wt% Sc [2], and Al-2 wt% Mg-0.2 wt% Sc, where both alloys were aged at 300 °C for 24 h.

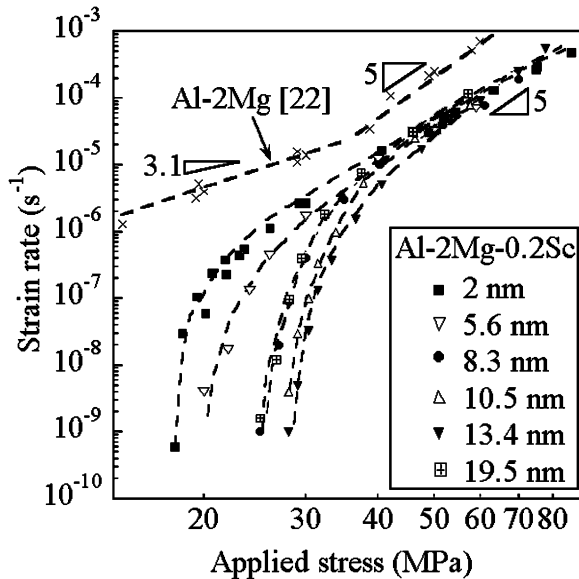


Fig. 6. Strain rate versus applied stress curves at 300 °C for Al-2wt% Mg [25] and Al-2 wt% Mg-0.2 wt% Sc alloys aged to produce different precipitate average radii.

## 4. Discussion

### 4.1. Room temperature strength

The presence of 2 wt% Mg introduces a significant solid-solution strengthening effect, which is observed in the as-quenched state. The microhardness value of the quenched binary Al-0.2 wt% Sc alloy is 220 MPa, whereas the hardness of the quenched Al-2 wt% Mg-0.2 wt% Sc alloy is double that value (439 MPa), which is comparable to handbook data for Al-2wt% Mg [11]. The superposition of the solid-solution and precipitate strengthening effects is given by Nembach [1]:

$$\Delta\sigma_{\text{total}} = (\Delta\sigma_{\text{ss}}^n + \Delta\sigma_{\text{p}}^n)^{1/n}, \quad (1)$$

where  $n$  lies between 1 and 2, implying that a linear superimposition of strengthening effect is an upper bound for the alloy strength. The linear superposition of the two strengthening effects is shown by the dashed lines in Fig. 4; the slightly higher strengthening effect observed in the ternary alloy (about 50 MPa) is within the experimental error for the measurement of the two alloy strengths and may be attributed to small concentration variations

in the alloys. The sharp increase in hardness occurs earlier for the ternary alloy, which is attributed to heterogeneous nucleation of  $\text{Al}_3\text{Sc}$  precipitates on Mg clusters; this is suggested by the presence of Mg at the center of the  $\text{Al}_3\text{Sc}$  precipitates, as measured by three-dimensional atom-probe (3DAP) microscopy [12].

The precipitate size dependence of the yield strength of the Al-Mg-Sc alloy (estimated by dividing the hardness by a factor of 3 [13]) is shown in Fig. 7. The critical radius for the transition from precipitate shearing to dislocation Orowan looping is evaluated using theoretical models [14–16] for the strengthening contributions due to shearing of the ordered precipitates ( $\Delta\sigma_1$ ), lattice mismatch ( $\Delta\sigma_2$ ), modulus mismatch ( $\Delta\sigma_3$ ), and to dislocation bypassing of the precipitates by the Orowan mechanism ( $\Delta\sigma_{\text{Or}}$ ), as described for the Al-Sc binary alloy in Ref. [2]. The highest values of  $\Delta\sigma_1$  and  $\Delta\sigma_2 + \Delta\sigma_3$  determine the strength of this alloy at small precipitate radii; at larger radii, the Orowan mechanism is controlling, when its strengthening contribution is smaller than that of the shearing mechanism. The parameters used in these calculations are: (a) the mean matrix orien-

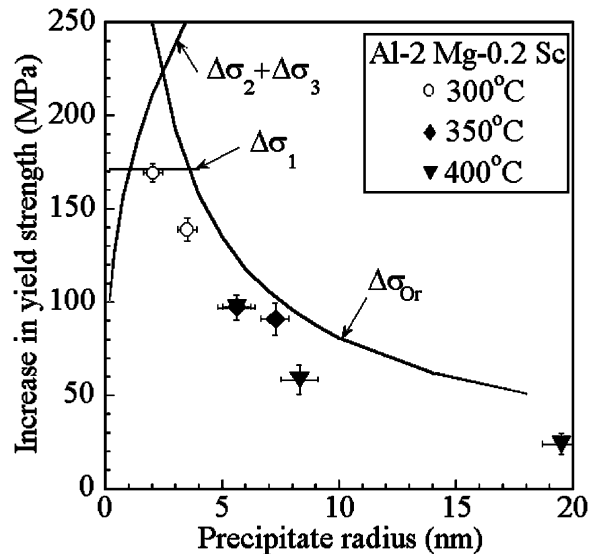


Fig. 7. Increase in Vickers microhardness versus average precipitate radius for Al-2 wt% Mg-0.2 wt% Sc aged to produce different average precipitate radii. Calculated curves are for an Al-0.2 wt% Sc alloy using equations of Ref. [2].

tation factor for aluminum,  $M = 3.06$  [17]; (b) the magnitude of the matrix Burgers vector,  $b = 0.286$  nm [18]; (c) the volume fraction of  $\text{Al}_3\text{Sc}$  precipitates,  $f = 0.53\%$  [19]; (d) an average value of the  $\text{Al}_3\text{Sc}$  antiphase boundary (APB) energy for a  $\{111\}$  plane taken from several reported values,  $\gamma_{apb} = 0.5$  J/m<sup>2</sup> [20–22]; (e) the matrix Poisson's ratio,  $\nu = 0.34$  [17]; and (f) the shear modulus of Al at room temperature,  $G = 25.4$  GPa [11,18]. These quantities are assumed unchanged by the addition of 2 wt% Mg. The constrained lattice parameter mismatch,  $\varepsilon = (2/3)(\Delta a/a)$ , where  $\Delta a/a$  is the fractional lattice parameter mismatch at room temperature, which decreases from 0.91% to 0.74% by addition of 2 wt% Mg [23].

As was the case for the binary Al–Sc alloys reported in Ref. [2], theoretical predictions for the dislocation looping mechanism are in reasonably good agreement with the experimental values for the ternary the Al–Mg–Sc alloy. The low experimental strength obtained at the smallest radius ( $r = 2$  nm) may be explained by the broad precipitate radius distribution with an average value  $r$  (coarsening of the precipitates) leading to an overall smaller yield strength value than that of a precipitate population with a unique radius  $r$ . An optimal precipitate radius of 2.4 nm is calculated for this ternary alloy, which is 15% larger than the critical radius for the Al–Sc alloys (2.1 nm), due to the decrease in lattice mismatch.

#### 4.2. Creep strength (high-stress regime)

As shown in Fig. 6, for stresses above 50 MPa, the stress exponent of the ternary alloy ( $n = 5$ ) is similar to that for the binary Al–2 wt% Mg alloy ( $n = 5.1$ , for the same stress range [25]), which is indicative of dislocation climb as the rate controlling deformation mechanism. Considering that all specimens deform at the same rate for a given stress independent of the average precipitates radius, it appears that the matrix behavior controls creep deformation in the high stress regime. The higher strength observed for the ternary alloy compared to the binary Al–Mg alloy may be due to precipitate bypass through the Orowan dislocation looping mechanism or to the grain texture produced by directional solidification, which affects

the Taylor factor and thus the creep strength in tension or compression [24].

#### 4.3. Creep threshold stress (low-stress regime)

##### 4.3.1. Coherent precipitates

At low strain rates, the markedly improved creep resistance of the Sc-containing alloys, as compared to pure aluminum (Fig. 5), suggests a strong interaction between  $\text{Al}_3\text{Sc}$  precipitates and mobile dislocations. Similarly to the binary Al–Sc alloys [2], the high and variable creep exponents ( $n = 5$ –40, Fig. 5) of the present ternary alloy are interpreted as resulting from a threshold stress,  $\sigma_{th}$ , below which creep rates,  $\dot{\varepsilon}$ , are negligible, resulting in a modified power-law equation [26]:

$$\dot{\varepsilon} = A \frac{D G b}{k_B T} \left( \frac{\sigma - \sigma_{th}}{G} \right)^n \quad (2)$$

where  $A$  is the Dorn constant,  $n$  the matrix stress exponent [18],  $D = D_o \exp(-Q/RT)$  is the diffusivity of Al in the matrix, where  $Q$  is the activation energy for diffusion,  $k_B$  is Boltzmann's constant, and  $\sigma$  is the applied stress.

Values for the threshold stress are obtained by plotting  $\dot{\varepsilon}^{1/n}$  versus  $\sigma$ , as shown in Fig. 8, with the intercept corresponding to the threshold stress value. A choice of  $n = 3$  was motivated by the fact that the behavior of Al–2 wt% Mg is characterized by  $n \sim 3$  for stresses below 30 MPa [25], and the threshold stress values are less than 30 MPa. The linearity of the best-fit curves is also better for  $n = 3$  than for  $n = 5$  at the lowest stresses (Fig. 8). The possible mechanisms considered to explain the presence of threshold stresses in precipitation- or dispersion-strengthened metals [26] are precipitate shearing, Orowan dislocation looping, dislocations climbing over precipitates, and dislocation detachment from precipitates (the latter mechanism is inoperative for coherent precipitates). The increase in strength due to Orowan dislocation looping around precipitates or to precipitate shearing mechanisms is estimated following Ref. [2], using  $f = 0.53\%$  as the volume fraction of  $\text{Al}_3\text{Sc}$  precipitates in the Al–2 wt% Mg matrix [19], and  $\Delta a/a = 0.83\%$  as the lattice parameter mismatch at 300 °C between  $\text{Al}_3\text{Sc}$  and Al–2 wt% Mg [23,27,28]. Values for the Orowan stress for the different aging

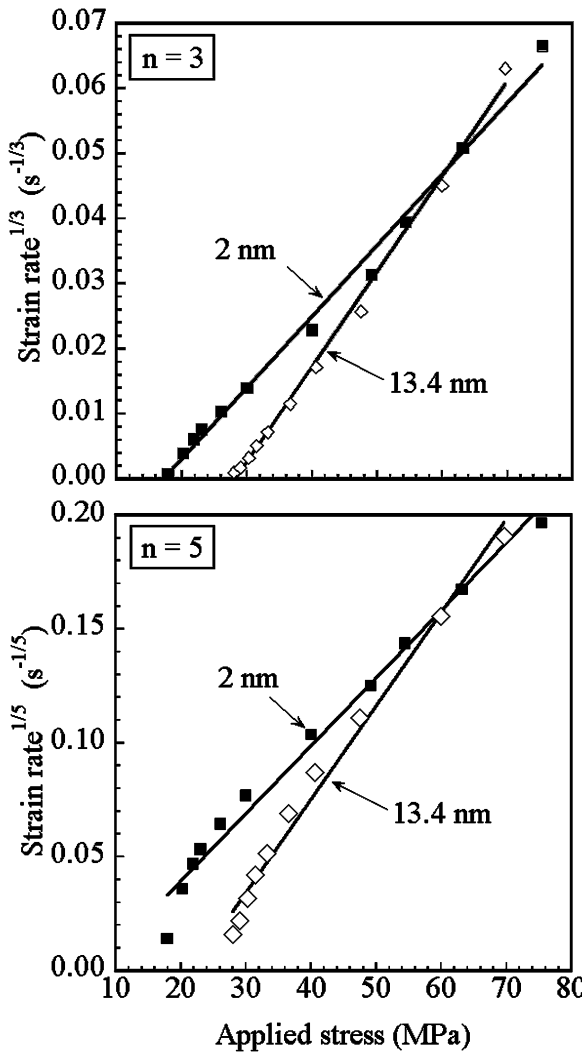


Fig. 8. Strain rates raised to the power 1/3 or 1/5 versus applied stress curves for an Al-2 wt% Mg-0.2 wt% Sc alloy aged at 300 °C for 24 h ( $\langle r \rangle = 2.0$  nm, solid squares) and at 300 °C for 24 h followed by 400 °C for 72 h ( $\langle r \rangle = 13.4$  nm, open symbols).

treatments are displayed in Table 1, showing that the Orowan dislocation looping mechanism would require much larger stresses than the creep threshold stresses we measured. The same conclusion is reached for the stress due to precipitate shearing, which is also calculated following Ref. [2], using Ref. [15]. The absence of TEM evidence for precipitate shearing supports the climb mechanism as

the operating bypass mechanism, as previously observed for binary Al-Sc alloys [2].

For comparison with the data, we obtained on binary Al-Sc alloys [2], the normalized threshold stress, defined as the ratio of the measured threshold stress to a calculated Orowan stress, is plotted as a function of average precipitate radius in Fig. 9. The experimental values of the normalized threshold stress increasing with increasing precipitate radius, is not predicted by the model of dislocations climbing over non-interacting precipitates developed by Rösler and Arzt [29]. Predictions from a recent model [30], however, taking into account elastic interactions between precipitates and climbing dislocations are in semi-quantitative agreement with the experimental data for average precipitate radii less than 15 nm. The normalized threshold stress data for the binary Al-Sc alloys [2] and of the present ternary alloy are also very similar, demonstrating that the presence of 2 wt% Mg has a negligible effect on the climb-bypass mechanism. This result was not anticipated since the reduction of the lattice parameter mismatch by the presence of Mg diminishes the elastic interactions between dislocations and precipitates, resulting in a noticeable decrease in the normalized threshold stress predicted by the model described in Ref. [30], as displayed in Fig. 9. This decrease due to adding Mg is not present in the data, possibly because of other microstructural parameters being affected by an Mg addition, e.g., diffusion constant, precipitate morphology, and segregation at the  $\alpha$ -Al/Al<sub>3</sub>Sc interface [31]. Changes in diffusion coefficients for the operative creep mechanism do not affect the athermal threshold stress. A change in morphology of an Al<sub>3</sub>Sc precipitate (from faceted to spheroidal) is not expected to cause a significant effect on the strength, due to the small extent of these morphological changes compared to the dimensions of the precipitates. Finally, the effect of Mg segregation at the  $\alpha$ -Al/Al<sub>3</sub>Sc interface on dislocation bypass is also assumed to be small, due to the very narrow width of the segregation peak at the  $\alpha$ -Al/Al<sub>3</sub>Sc interface (less than 2 nm) [31]. Dislocations are anticipated to stand-off farther away from the interface than the width of the segregated region, because of the nature of the elastic interaction with the precipi-

Table 1

Dependence on aging-treatment conditions, average precipitate radius,  $r$ , and inter-precipitate spacing,  $\lambda$ , of the experimental threshold stress,  $\sigma_{th}$ , calculated Orowan stress,  $\sigma_{Or}$ , and calculated yield stress for a precipitate shearing mechanism,  $\sigma_{sh}$ , all at 300 °C

Heat-treatments	$r$ (nm)	$\lambda^a$ (nm)	$\sigma_{th}$ (MPa)	$\sigma_{Or}^b$ (MPa)	$\sigma_{sh}^c$ (MPa)
300 °C, 24h	2.0	39	18	199	205
300 °C, 24 h+400 °C, 2 h	5.6	109	20	99	283
300 °C, 24 h+400 °C, 10 h	8.3	161	24	74	321
300 °C, 24 h+400 °C, 24 h	10.5	204	29	61	346
300 °C, 24 h+400 °C, 72 h	13.4	261	27	51	374
300 °C, 24h+400 °C, 240 h	19.5	379	25	38	423
300 °C, 24 h+400 °C, 280 h+450 °C, 4 h	25	486	21	31	459

<sup>a</sup> From Eq. (6) in Ref. [2].

<sup>b</sup> From Eq. (5) in Ref. [2] (calculated at 300 °C).

<sup>c</sup> From Eqs. (2)–(4) in Ref. [2] (calculated at 300 °C).

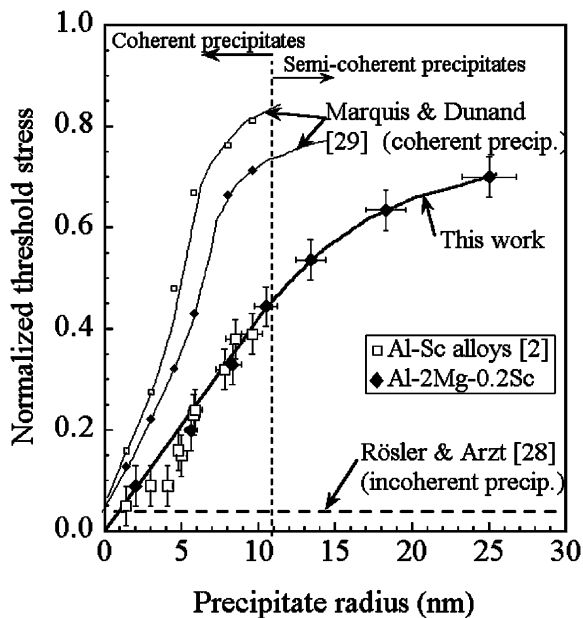


Fig. 9. Creep threshold stress, normalized with respect to a calculated Orowan stress at 300 °C, as a function of average precipitate radius for Al–2 wt% Mg–0.2 wt% Sc (filled symbols) and binary Al–0.1–0.3 wt% Sc alloys (open symbols, from Ref. [2]), aged at different temperatures. Experimental data are compared to predictions of a general climb model without elastic interactions [29] and with elastic interactions for both binary and ternary alloys [30].

tates, so climb can be assumed to take place in a matrix with an average composition of 2 wt% Mg.

#### 4.3.2. Semi-coherent precipitates

Because the lattice mismatch at 300 °C is reduced from 1.08% for a binary Al–Sc alloy to 0.83% for a ternary Al–2 wt% Mg–Sc alloy, the calculated critical precipitate radius for coherency loss is increased from 9 to 11 nm (obtained when the number of lattice planes multiplied by the lattice misfit is equal to one lattice spacing). This value is in reasonable agreement with the value  $\langle r \rangle \approx 15$  nm estimated earlier employing TEM observations. The model described in Ref. [30] is strictly for coherent precipitates and cannot be used to predict the normalized threshold stress for precipitate radii beyond the coherency limit. For fully incoherent particles without elastic interactions with dislocations, the model of Rösler and Arzt [29] predicts a normalized threshold stress of ca. 2%. A possible explanation for the unexpectedly high normalized threshold stress values (greater than 60%) when precipitates lose coherency is the residual elastic interactions due to the modulus and the lattice mismatch effects, which are only partially relaxed by the presence of interfacial misfit dislocations. These misfit dislocations also interact elastically with the matrix dislocations, bypassing the precipitates, by blocking their climb motion. The effect of interfacial misfit dislocations would

be similar to that of the elastic interactions previously described [2], i.e., the interfacial misfit dislocations create an additional force acting on moving dislocations. For the average precipitate radii considered in this study, 15–25 nm, one to two interfacial dislocations are expected at the matrix/precipitate interface. More research is needed to test this hypothesis.

## 5. Conclusions

This study examined the relationships between the microstructural and mechanical properties of an Al–2 wt% Mg–0.2 wt% Sc alloy strengthened by Mg in solid-solution and Al<sub>3</sub>Sc nanoscale precipitates. Aging between 300 and 450 °C resulted in spheroidal Al<sub>3</sub>Sc precipitates with an average radius between 2 and 25 nm. Microhardness values obtained after aging at 300 and 350 °C indicate that the alloy's strength results from the superposition of solid-solution strengthening and precipitate strengthening. Solid-solution strengthening due to Mg contributes to an increase in strength of about 75 MPa and a peak strength (ca. 310 MPa) is obtained for a mean precipitate radius of about 2.5 nm. The increase in strength due to Al<sub>3</sub>Sc precipitates follows the classical predictions of dispersion-strengthening theory.

As compared to the binary Al–0.2 wt% Sc alloy, without solid-solution strengthening, the ternary alloy is more creep resistant at high stresses, where the stress exponent is  $\approx 5$ , and the strain rate is independent of the average Al<sub>3</sub>Sc precipitate radius. At small applied stresses, a threshold stress is present that increases with increasing precipitate radius. The magnitude of the threshold stress and its dependence on the average precipitate radius are similar to those measured for binary Al–Sc alloys. The threshold stress increases from 9% to 70% of the Orowan stress for dislocation looping with increasing average Al<sub>3</sub>Sc precipitates radius from 2 to 25 nm. An existing model [30], which considers the dislocation climb-bypass mechanism in the presence of elastic interactions between dislocations and coherent precipitates, is in semi-quantitative agreement with the average precipitate radius dependence of the threshold stress, up to an aver-

age radius of  $\sim 12$  nm. For larger average radii, the precipitates are semi-coherent and the model is not applicable; the measured threshold stress remains high, however, probably because of elastic interactions between the bypassing dislocations and interfacial misfit dislocations at  $\alpha$ -Al/Al<sub>3</sub>Sc interfaces.

## Acknowledgments

This research is supported by the United States Department of Energy, Basic Sciences Division, under contract DE-FG02-98ER45721. The authors acknowledge Alcoa Inc. and Ashurst Inc. for kindly supplying the Al–Sc master alloys.

## References

- [1] Nembach E. Particle strengthening of metals and alloys. New York: John Wiley, 1997.
- [2] Marquis EA, Seidman DN, Dunand DC. Acta Mater 2002;50:4021.
- [3] Yavari P, Langdon TG. Acta Metall 1982;30:2181.
- [4] Yavari P, Mohamed F, Langdon T. Acta Metall 1981;29:1495.
- [5] Hong SI. Scripta Metall 1984;18:1351.
- [6] McNelley T, Michal D, Salama A. Scripta Metal 1989;23:1657.
- [7] Mohamed FA, Langdon T. Acta Metall 1974;22:779.
- [8] Mohamed FA. Mater Sci Eng 1998;245:242.
- [9] Oliver WC, Nix WD. Acta Metall 1982;30:1335.
- [10] Kikuchi S, Uesugi M, Koiwa M. Strength of metals and alloys (ICSMA 8). Proceedings of the Eighth International Conference, Finland, vol. 2. 1988. p. 525.
- [11] ASM, editor. Metals handbook, vol. 2. Materials Park (OH), 1990.
- [12] Marquis EA, Seidman DN. Ultramicroscopy 2003; to appear.
- [13] Tabor D. The hardness of metals. New York: Oxford University Press, 1951.
- [14] Brown LM, Ham RK. In: Kelly A, Nicholson RB, editors. Strengthening Methods in Crystals. Amsterdam: Elsevier; 1971. p. 9.
- [15] Ardell AJ. Metall Trans A 1985;16:2131.
- [16] Schleisier C, Nembach E. Acta Metall Mater 1995;43:3983.
- [17] Meyers MA, Chawla KK. Mechanical metallurgy: principles and applications. Englewood Cliffs, NJ: Prentice Hall; 1984.
- [18] Frost HJ, Ashby MF. Deformation mechanism maps. Oxford: Pergamon Press, 1982.

- [19] Murray JL. Private communication, 2002.
- [20] Fu CL. *J Mater Res* 1990;5:971.
- [21] George EP, Pope DP, Fu CL et al. *ISIJ Intern* 1991;31:1063.
- [22] Fukunaga K, Shouji T, Miura Y. *Mater Sci Eng A* 1997;239:202.
- [23] JCPDS—International Centre for Diffraction Data, v. 2.00 (1998).
- [24] Jansen AM, Dunand DC. *Acta Mater* 1997;45:4583.
- [25] Oikawa H, Sugawara K, Karashima S. *Scripta Metall* 1976;10:885.
- [26] Cadek J. *Creep in metallic materials*. New York: Elsevier, 1998.
- [27] Hatch JE. *Aluminum: properties and physical metallurgy*. Metals Park (OH): ASM, 1984.
- [28] Harada Y, Dunand DC. *Scripta Mater* 2002;48:219.
- [29] Rösler J, Arzt E. *Acta Metall* 1988;36:1043.
- [30] Marquis EA, Dunand DC. *Scripta Mater* 2002;47:503.
- [31] Marquis EA, Seidman DN, Asta M, Woodard CM, Ozolins V. *Phys Rev Lett* (2003) (to appear)